Paper published as

Tancredi, U. & D'Errico, M. (2003), 'Solar Array Configurations for Microsatellites Flying in Sunsynchronous Orbits''Proceedings of the 2003 IEEE Aerospace Conference', 2573-2586.

DOI: 10.1109/AERO.2003.1235184

Solar Array Configurations for Microsatellites Flying in Sunsynchronous Orbits

Urbano Tancredi
Aerospace and Mechanical Engineering Department
Seconda Università degli Studi di Napoli
Via Roma 29
81031, Aversa (CE)
+39-081-5010285
urbano.tancredi@unina2.it

Marco D'Errico
Aerospace and Mechanical Engineering Department
Seconda Università degli Studi di Napoli
Via Roma 29
81031, Aversa (CE)
+39-081-5010223
marco.derrico@unina2.it

Abstract—A beginning of life maximum power point, solar array power output model is developed to comparatively evaluate different kind of array configurations. To correctly describe temperature effects on power output, various thermal models are compared, selecting the better one with respect to solar panel type. Two different constant-temperature thermal models are selected in order to describe body mounted and sun pointing solar arrays. Various body mounted solar arrays configurations are compared to sun pointing ones for sunsynchronous orbits with ascending node local time ranging from 12 to 6 am. To this end, total solar array area, power time history and satellite volume are considered. Results show that configurations with one or three body mounted panels can adequately replace a sun pointing array depending on the ascending node local time.

TABLE OF CONTENTS

1. INTRODUCTION

In the last two decades, spacecraft mass and power have been increasingly limited to reduce costs, risks, and development time, often at the expense of performance. Microsatellites were first used for radio amateur communications and technological demonstrations (AMSAT, UOSAT). Subsequently they have been found to be useful in a large variety of applications (see reports of the conferences by AIAA/USU, IAA, CNES). Because of lower costs, microsatellites can allow frequent re-flight and use in constellations/formations. As a consequence, more emphasis has been given to the potential of using microsatellites for Earth observation by synthesizing large advanced sensors using simpler instruments distributed on different satellites flying in formation [1],[2]. New technology plays a fundamental role in enabling high performance, which can be vital when implementing such missions. With regards to the electrical power subsystem (EPS), great improvements have been obtained in power output, storage, and control: for example, triple-junction cells (26.8% efficiency), Li-Ion batteries (high Wh efficiency and power density), and new DC/DC converters (94% efficiency). In this context, the Universities of Naples have been working on microsatellite technology integration since 1997 [3],[4] under contract with the Italian Space Agency. Presently, a microsatellite bus for formation flying application is under study and the authors are involved in EPS design.

As far as photovoltaic power output is concerned, power and thermal designs are thoroughly interdependent, since EPS performance influences the operating temperature which impacts photovoltaic power output. In addition, power/thermal design performance can drive configuration

[1] 0-7803-7651-X/03/$17.00/© 2003 IEEE
[2] IEEEAC paper #1033, Updated December 19, 2002

selection: e.g. body mounted solar panel, deployable solar wings, deployable wings and pointing mechanisms, panel dimensions and so on. These interactions can become even more critical when small platforms are considered due to a reduced design flexibility. Anigstein and Sanchez Peña thoroughly analyzed solar panel orientation versus generated power, but they did not considered the operating temperature as a design variable. D'Errico and Pastena [3] analyzed the effect of equilibrium temperature on solar array power output, determining the best panel deployment angles for a microsatellite application.
In this paper a solar array performance analysis which takes into account orbit characteristics, solar array-sun relative orientation, and solar array temperature along the orbit is presented. In particular, a thermal model is studied, which, for each position along the orbit considers the heat flux coming from the Sun and the Earth (albedo and emission), the output flux of the solar array, and the photovoltaic power output (maximum power point). Steady-state and non-stationary solutions are analyzed for body-mounted and deployed solar panels to identify a thermal model suitable for power design. To this end, Sun and Earth positions with respect to the solar array-fixed reference frame, surface thermal properties, solar cell thermal properties and efficiency are considered. Then, the maximum solar panel power is computed at beginning of life (BOL), considering efficiency dependence on temperature and effective Sun direction.
The model is applied to compare different solar array configurations for microsatellites flying in sunsynchronous orbits. In particular, deployable, sun-pointing arrays and a number of body-mounted configurations are analyzed as a function of the ascending node local time. Identification of the best option is carried out considering the solar array area as the parameter to be minimized. In addition, satellite volume and uniformity of power generation are evaluated as second-level parameters to confirm the configuration selection. It is worth noting that, as outlined in [4] and [5], uniformity of power output along the orbit is an important property which guarantees useful power utilization, in particular with reference to battery charge.

2. MODEL ASSESSMENT

The model described in this paper computes the maximum power P_U that a solar array (SA) can deliver to the Electric Power Subsystem (EPS). According to the formulation given in [6], P_U has the following functional expression:

$$P_U = P_I A_P \eta \qquad (1)$$

where P_I is the incident power on the solar array per square meter, A_P is the total area covered by solar cells and η is their average efficiency.
The panel's illumination conditions are taken into account by means of P_I, while η conveys solar cells electrical characteristics and temperature effects (ageing is not included in this analysis).

Efficiency η Model

Assuming a linear dependency on temperature [7], the solar cell efficiency has been described as:

$$\eta = \eta_0 \cdot \left[1 + K_T \cdot \Delta T_0\right] \qquad (2)$$

where η_0 is the efficiency value under standard nominal conditions [8], ΔT_0 is the difference between actual and nominal temperature and K_T is a constant cell parameter. Even though the values of K_T are generally small, typically $K_T \approx 2 \cdot 10^{-3}$ for Ge-based cells, temperature effects on cell efficiency are not negligible [7].

A general thermal energy balance of a deployed solar array can be written as:

$$P_{AB} - P_U\left(T\right) - P_{EM}\left(T^4\right) = mc_P \frac{dT}{dt} + q_{CPL} \qquad (3)$$

The temperature (T) dependencies are explicit for the sake of clarity, P_{AB} is the absorbed thermal power, P_{EM} is the thermal emitted power, m and c_P are array's mass and specific heat respectively; q_{CPL} is the thermal flux between the array and satellite's primary structure, consisting of both conductive and radiative contribution.
Due to temperature dependency of Equations (2) and (3), a thermal model is required. A number of different formulations can be found to simulate and/or characterize solar panels [9],[10],[11]. Because of their aims, they are generally complex, requiring a schematization of the solar panel and satellite bus in details. As far as preliminary design is concerned, thermal models existing in literature can be sorted as follows:

- Transient–coupled model [12],[13], obtained considering all the terms in (3).
- On-orbit steady-state model [3], neglecting the right hand side of (3).
- Constant array temperature [14];[15].

The transient–coupled model is the most accurate and complex, needing the knowledge of both solar array thermal capacity and array–satellite thermal coupling characteristics. On the other hand, a realistic estimate of these parameters is possible if array's structure, material, and configuration are at least preliminary defined. Therefore, simpler models are to be preferred, which are better suited for applications to the configuration design, when no enough details are available.

Nevertheless, the transient model, thanks to its higher accuracy, can be used to define a reference solution in order

to evaluate the accuracy of the two simpler thermal models. To this end, the following unlikeness indexes are defined:

$$J = \frac{\int_{t_{ill}} |\eta - \eta_R| \, dt}{\int_{t_{ill}} \eta_R \, dt} \tag{4}$$

$$J_m = \frac{\int_{t_{ill}} \eta dt - \int_{t_{ill}} \eta_R \, dt}{\int_{t_{ill}} \eta_R \, dt} \tag{5}$$

where the subscript R refers to reference conditions, i.e. considering array's transient temperature. Since we're interested in temperature effects on P_U, and $P_U \equiv 0$ in eclipse, the above integrals are restricted to the sunlit portion of the orbit (t_{ill}).
J and J_m quantify the accuracy of deviation of η–computation when steady-state temperature or constant temperature models are considered with reference to the transient–coupled formulation. It is worth noting that delivered energies (or, equivalently, mean powers) drive array size. Therefore, using Equation (5), J_m can be interpreted as the relative deviation of array area which is caused by the thermal approximation. In addition, J represents the deviation in solar cell's electrical behavior on the sunlit portion of an orbit.

In conclusion, the more suitable thermal model is selected by comparing the unlikeness indexes, identifying the option with smaller deviations w.r.t. the solution obtained with the transient–coupled formulation.
The analysis is conducted for two solar array categories: sun pointing (SP) and body mounted (BM). For the purpose of selecting and validating the thermal model a test case is considered, consisting in a small cubic satellite (40 cm side length), in sunsynchronous 12 am–12 pm circular orbit at an altitude of 800 Km.

Sun Pointing Solar Arrays—In order to compute the reference transient–coupled temperature profile, array's thermal capacity and array–satellite thermal coupling must be estimated. To conservatively enhance the difference between models, i.e. overestimate the loss of accuracy, these parameters have been fixed at the higher realistic values for SP arrays. To this end, a conventional aluminum honeycomb rigid structure has been selected, leading to a specific heat value of 945 J/KgK [16] and a unit area mass of 2,74 Kg/m^2 [12]. The coupling factors have been computed according to [16].
Then, the three thermal models have been used to calculate the temperature profiles along an orbit. For the constant temperature model, the steady-state temperature is evaluated and then averaged over the sunlit part of the orbit:

$$T_M = \left[\frac{1}{A_P \left(\varepsilon_{fr} + \varepsilon_{re} \right) \sigma} \frac{1}{t_{ill}} \int_{t_{ill}} \left(P_{AB} - P_U \right) \bullet dt \right]^{1/4} \tag{6}$$

where ε_{fr} and ε_{re} are array's front and rear mean infrared emissivities, and σ is the Stefan – Boltzmann constant.
Figure 1 and Figure 2 show, in two different scales each, temperature and efficiency time histories, as functions of the true anomaly ν. The main contribution to the difference between models is the overshoot in power output when exiting the eclipse, as it can be seen in Figure 2. Results also show a phase delay between transient and steady-state temperature profiles, underlining how, even after the initial mismatch recovery, the steady-state description introduces an approximation not significantly better than the constant value model.

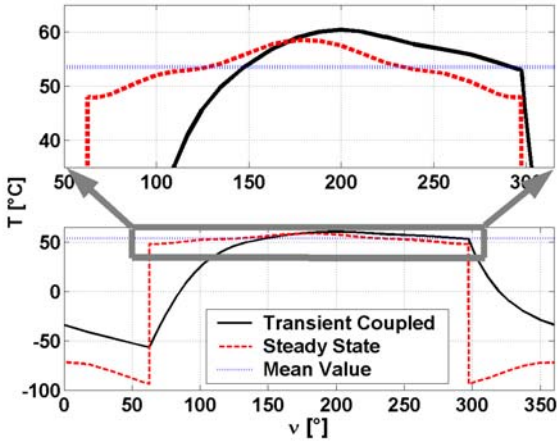

Figure 1 - Temperature time-histories of various sun pointing solar arrays thermal models.

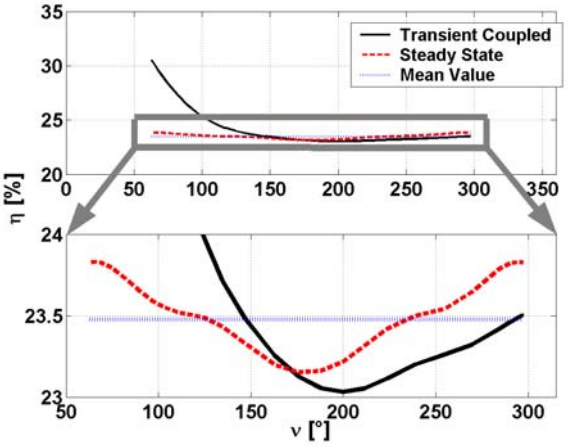

Figure 2 - Efficiency time-histories of various sun pointing solar arrays thermal models.

These considerations are definitely confirmed by the computation of the unlikeness indexes (Table 1). It is worth

pointing out that their values are well under the typical model accuracies discussed in [6]. In addition, since they are similar for both models, the constant value one, with temperature defined by Equation (6), is selected for describing sun pointing solar arrays.

Index	Steady State	Mean Value
J (%)	3,70	3,94
J_m (%)	-2,57	-2,59

Table 1 - SP thermal models comparison.

Body Mounted Solar Arrays— Because of the intimate connection with the satellite's bus, body mounted solar arrays can be assumed at the same temperature of the whole satellite, supposed isothermal. The reference transient–coupled parameters have been fixed according to the microsatellite configuration described in [17].

Since a satellite bus has a thermal capacity much larger than a solar array, a larger discrepancy between transient and steady–state temperature profiles can be foreseen, with larger differences occurring when the satellite comes to sunlight from the eclipse. Therefore, in order to reduce the unlikeness indexes values, the constant temperature model is built on the steady-state temperature averaged over the whole orbit, including both the sunlit and the shadowed orbit arcs:

$$T_M = \left[\frac{1}{A_S \varepsilon_S \sigma} \frac{1}{t_{ORB}} \int_0^{t_{ORB}} \left(P_{AB} + \overline{P_U} \right) \bullet dt \right]^{1/4} \qquad (7)$$

where A_S is satellite surface's extension, ε_S is its mean infrared emissivity, P_U is supposed to be uniformly dissipated in the orbit, and t_{ORB} is the orbital period.
Figure 3 shows temperature and efficiency time histories, as functions of the true anomaly ν. The beneficial effect of averaging the steady-state temperature over the whole orbit is evident. Thus, the indexes values (Table 2) show a better agreement of the constant temperature model to the reference one than considering the isothermal satellite in steady-state conditions. However, it is worth pointing out that using the proposed constant temperature leads to an underestimate of array size, as revealed by the corresponding positive value of J_m.

Index	Steady State	Mean Value
J (%)	4,72	2,68
J_m (%)	-4,66	1,31

Table 2 - BM thermal models comparison.

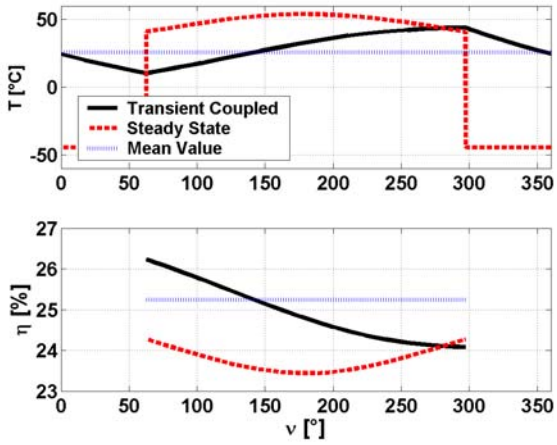

Figure 3 – Temperature and efficiency time-histories of various isothermal satellite thermal models.

Again, the loss of accuracy of the simpler formulation is well under the typical model accuracies [6]. Hence the constant value model is selected for describing body mounted solar arrays as well.

Conclusions—The above analysis has shown how:

- Sun pointing configurations can be adequately described considering the array always at the same temperature, as obtained in (6), considering the mean steady-state value in the orbit sunlit portion.
- Also body mounted configurations can be adequately described considering the panels always at the same temperature, but as obtained in (7), considering the steady-state value averaged over the whole orbit.

When solar array design is concerned, constant temperature models are frequently adopted, as it can be found in [6] and [19]. Between these two formulations, even though the thermal models are not explicitly described in details, some differences can be highlighted, specifically in the selected temperature values for BM solar panels. Because it isn't possible to radiate heat in deep space from the back side, [6] considers BM arrays warmer than SP ones. On the other hand, BM array temperatures computed by [19] are lower than those of SP arrays, due to the heat sink behavior of the satellite bus. The assumption, made in the present analysis (BM array temperature coincident with the isothermal satellite one) bears similarities with the approach of [19], leading to temperature values generally smaller than SP ones.

Incident Power P_I Model

The sunlight power incident on solar array active surface is computed as a sum of direct sunlight and reflected albedo radiation. Albedo contribution is calculated by means of numerically evaluated view factors, using standard formulation [6]. The cosine law of power output is used,

meaning that, besides albedo contribution, solar array's power output depends on the angle between the Sun vector **S** and panel's normal **p**.
To compute the projected angle of the Sun vector **S** on the solar panels for an arbitrary orientation we first define (X, Y, Z) a Geocentric Reference Frame (GRF), in whom the Sun vector is known through it's right ascension α and declination δ, that varies periodically in an year between $[-\delta_S,+\delta_S]$, where $\delta_S = 23.44$ °.
Then, the panel normal **p** is defined in (X_O, Y_O, Z_O) a Body-Fixed Reference Frame (BRF). We consider the case where the satellite body is fixed with respect to orbit's velocity and normal vectors, i.e., there are no significant attitude errors. Therefore the BRF is defined as follows: the Z_O axis is nadir pointing, Y_O is opposed to the orbit angular velocity $\boldsymbol{\omega_{ORB}}$ and the X_O axis is directed so as to form a right-handed set of coordinate axes. Given the coordinates of **p** in BRF and **S** in GRF the angle **pS** can be computed by means of Euler Rotation Matrices, univocally determined by the knowledge of the orbital parameters Ω, ν, and i.

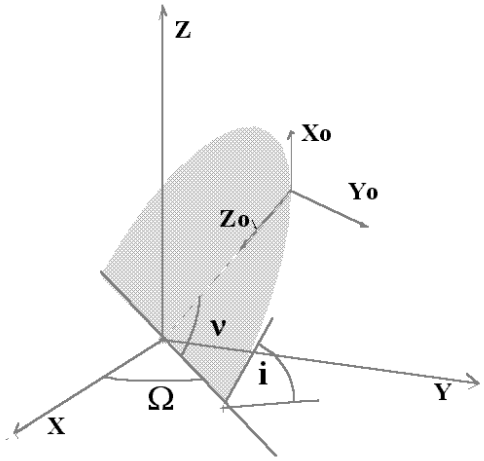

Figure 4 -Geocentric and Body Reference Frames.

The selected thermal/power model allows to determine the power orbital profile obtainable by a sun pointing (SP) or body mounted (BM) solar array, once chosen:

- Orbit
- Year's period, i.e. Sun vector in GRF.
- Solar cells technology and performance.
- Array configuration, in terms of sun pointing characteristics or a configuration of multiple body mounted panels.
- Solar array area (SP) / satellite dimensions (BM)
- Solar array rear side's surface finish (SP) / satellite's surface finish (BM)

The model can be used also in a reverse manner. By inspection of Equation (1), indeed, the knowledge of both efficiency value and incident power profile is sufficient to compute the solar array area A_P needed to satisfy a power requisite $P_U=P_{REQ}$.

3. PRELIMINARY ANALYSIS

We restrict our analysis to sunsynchronous circular orbits only. In particular, an altitude of 800 Km has been selected, leading to a sunsynchronous inclination of $i \approx 98.6$ [°]. Hence, from the sun-orbit relative orientation point of view, the orbit is univocally determined by the ascending node local time. From geometric considerations, the results obtained in a local time interval of 6 hours can be extended to all the possible 24 hours range. Therefore, in the present analysis the examined ascending node local time interval is [12 am, 6 am].

To gain insights into the impacts of the design variables on the performances of solar arrays, a preliminary analysis has been conducted. The performance attainable by a solar array can be evaluated from the energy it can deliver in an orbit to the EPS, or, equivalently, the on-orbit mean delivered power P_{MEAN}.
Apart from the dependencies of satellite bus temperature on the BM panels area, the P_U–A_P relation can be assumed as linear (1). For the sake of simplicity let us consider unit area solar panels in the ambit of preliminary analysis. Under this assumption, P_{MEAN} represent the mean power per square meter, that takes into account only P_I and η.
The incident specific power P_I depends on both the fraction of daylight in the orbit and the **pS** angle time history. For SP arrays, because of the identically zero **pS** angle, P_I attains a maximum, whose value depends on the orbit illumination conditions. The **p** vector of BM panels, instead, is fixed in the BRF, while the Sun vector **S** is not. This results in an additional reduction, besides that of eclipse, in the available P_I. The magnitude of this further performance loss depends mainly on the **p** orientation chosen. Thus, the orientation of BM panels is a critical design variable, whose worthiness can be evaluated comparing the resulting P_{MEAN} with that of SP arrays.
It is worth noting that energy is delivered only if the angle **pS** is less than 90° and the satellite isn't in eclipse. Therefore, panels which are apparently similar can behave in different manner. In fact, defining t_E as the eclipse time interval and t_{SH} as the time interval when the sun is behind the panel, the produced energy depends on the superimposing of these two time intervals. This considerations will be evident in the following, when panels with normal lying in the orbital plane will be compared.
To give an indication on optimal orientations, a set of five different **p** vectors is considered. With reference to the nomenclature defined in Figure 5, reserving the earth pointing face to the payload, we assume a configuration in which all the five available faces are covered by solar panels.

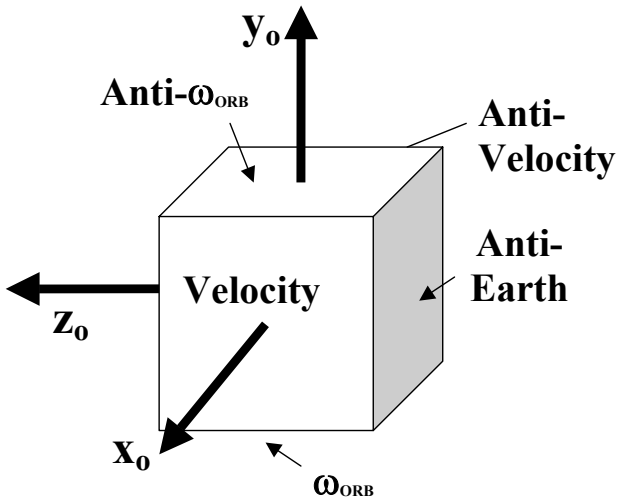

Figure 5 – Satellite's faces Nomenclature.

Hence, the comparison of the unit-area P_{MEAN} of each panel, referred to the SP value, gives indication on the effectiveness of the solar energy collection and conversion.
To give a better physical interpretation of the resulting values of P_{MEAN}, it is worth prior analyzing the apparent Sun motion in the BRF. Complex **S** trajectories result from the composition of the orbital motion and Earth's revolution around the Sun. However, in an orbit period, the Sun can be considered fixed in the GRF. Since the relative motion of the BRF w.r.t. the GRF is given by a rotation around Y_0 with ω_{ORB} angular velocity, **S** in one orbit describes a cone centered on the Y_0 axis. The cone semi-aperture depends on the relative orientation of the sun vector **S** and the orbit normal, i.e. from ascending node local time and year period.
Figure 6 to Figure 8 show, for three representative local times (noon, 9 am and 6 am) the sun vector motion in three peculiar year periods: Summer and Winter Solstices and an Equinox.

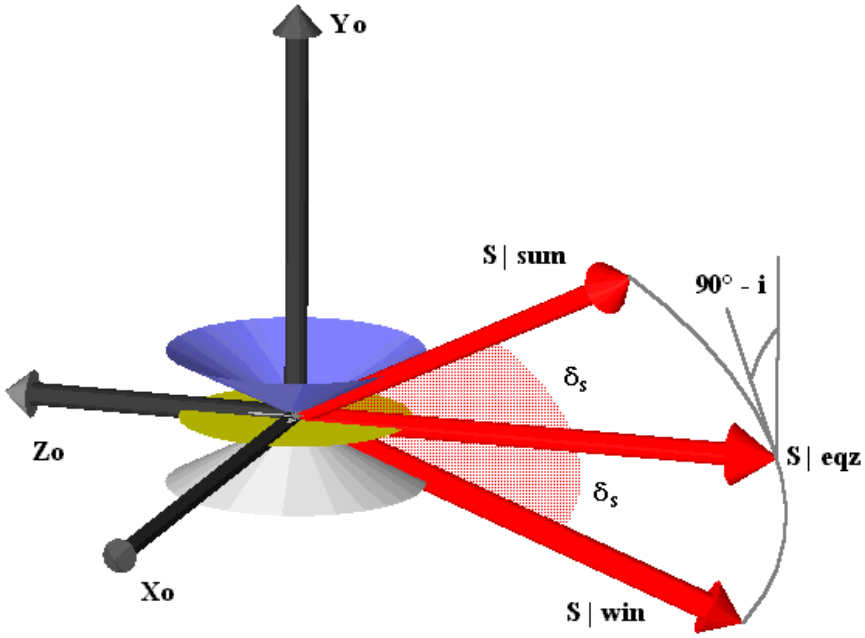

Figure 6 – Apparent Sun Motion In BRF for 12 am Orbit.

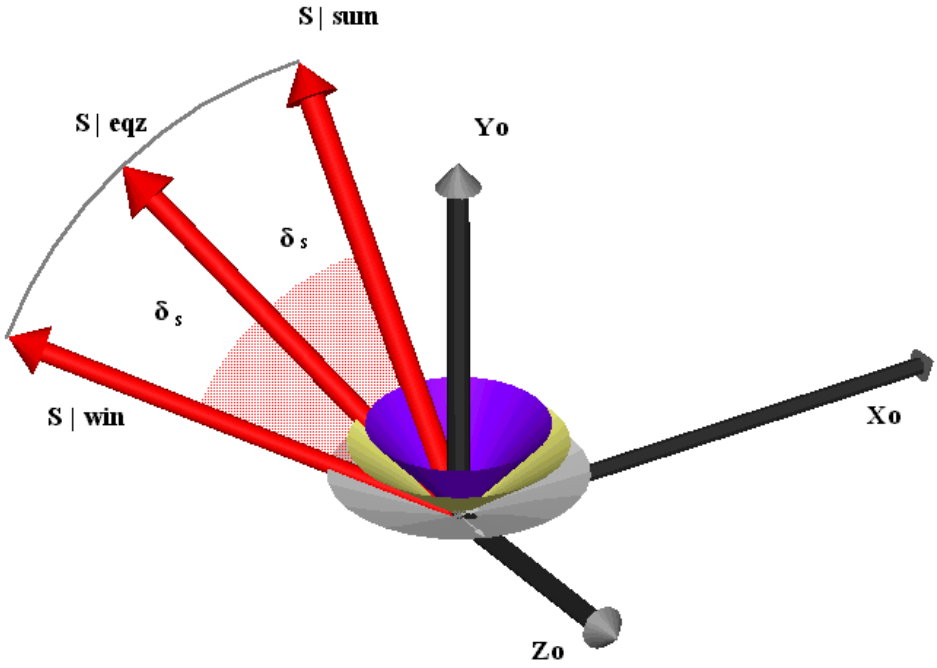

Figure 7 - Apparent Sun Motion In BRF for 9 am Orbit.

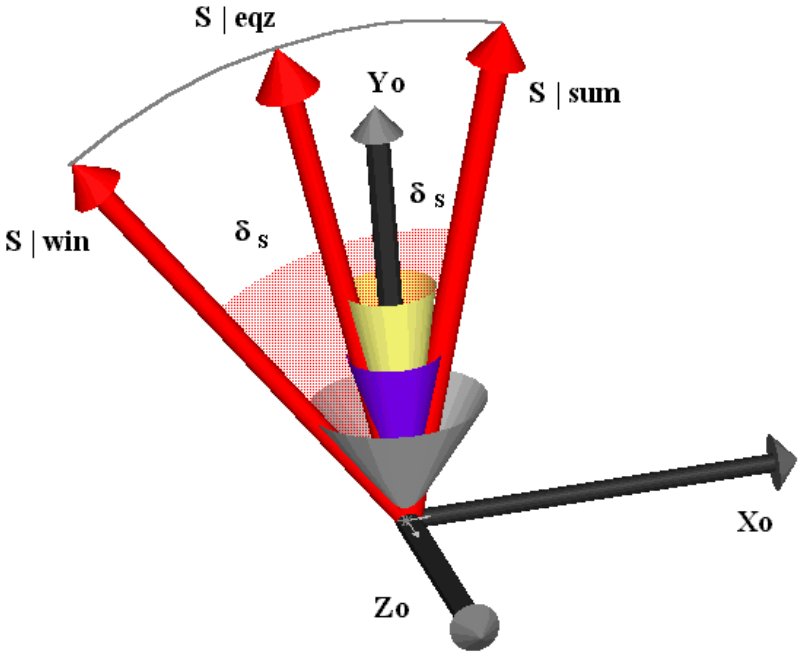

Figure 8 - Apparent Sun Motion In BRF for 6 am Orbit

For the 12 am orbit, because of the symmetry of the cones w.r.t. the orbital plane X_OZ_O a configuration of 3 BM panels {Velocity ; Anti-Earth ; Anti-Velocity} seems promising. Moving towards the 6 am orbit, due to the increasing narrowness of all the three cones we do expect a corresponding increasing power produced by the Anti-ω_{ORB} panel.

In order to verify these considerations and to preliminarily identify candidate configurations, an analysis has been conducted including also temperature effects, by means of the model outlined in Section 2. The results, that refer to

arrays with Improved Triple Junction solar cells (see details in Table 5), are collected in Figure 9 to Figure 11, that depict the P_{MEAN} vs. ascending node local time in three different year periods.

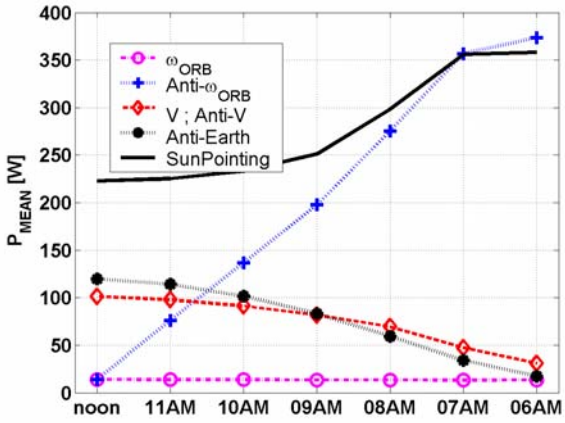

Figure 9 – Mean Delivered Power for various Orbits at Equinoxes; A_P=1 m^2.

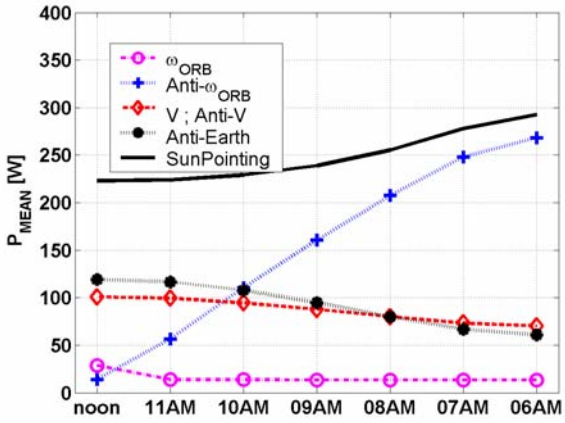

Figure 10 - Mean Delivered Power for various Orbits at Winter Solstice; A_P=1 m^2.

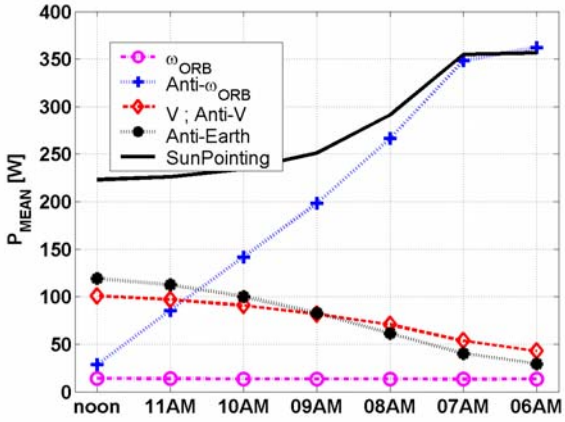

Figure 11 - Mean Delivered Power for various Orbits at Summer Solstice; A_P=1 m^2.

Some considerations on each available location can be outlined at this point:

- ω_{ORB} — Gives a very small contribution, compared to all the other panels, because it almost never collects direct sunlight in the examined local time range.

- Velocity and Anti-Velocity — Due to the symmetry of both the panel-Earth and the panel-Sun relative orientation, the overlapping of t_E and t_{SH} is equal. Hence, the two locations are completely equivalent. As we expected, a panel in this location is capable of deliver a relevant amount of power for 12 am orbits, rapidly decreasing its performance with changes in the local time towards 6 am.

- Anti-Earth — Due to the fact that it's normal lies in the orbital plane it has the same characteristics of the Velocity and Anti-Velocity locations, revealing a slightly better performance in 12 to 9 am orbits, because of the synchronization between the orbital motion (**pS** angle) and the eclipse occurring. For earlier local times, the delivered energies are smaller due to the absence of albedo contribution.

- Anti-ω_{ORB} — This location shows rapidly increasing performance moving from 12 to 6 am orbits, in whom at equinoxes and summer solstice it's capable of delivering even more energy than a sun pointing solar array of the same area. This unexpected phenomenon is due to the combining effects of both the temperature difference between BM's and SP, and the **pS** angle profile.

As shown in Table 3, in equinoxes and in summer the performance degradation induced by a non pointed panel are recovered by the relevant temperature difference. As already stated, the BM temperature depends by the solar cell area, i.e. from the satellite dimensions. Specifically, selecting an A_P value smaller (bigger) than one square meter diminishes (increases) both the emitting surface and the dissipated power. From Equation (3), these two effects tend to balance each other, limiting the approximation introduced by neglecting the temperature-BM array area dependency.

	SP Temperature [°C]	**BM Temperature [°C]**	**Anti-ω_{ORB} pS Angle [°]**
Equinox	49,56	27,64	8,60
Winter	52,71	31,08	32,04
Summer	49,89	31,74	14,84

Table 3 – Temperature and Pointing Difference Between Sun Pointing and Anti-ω_{ORB} Panels.

4. OPTIMAL CONFIGURATIONS

As already stated, the performance attainable by a solar array can be quantified by the power it can deliver to the EPS and, therefore, to the electrical loads.
Moreover the performance can be evaluated from two different points of view:

- The energy delivered in an orbit, or, equivalently, the mean delivered power P_{MEAN}, that gives indication on mean sunlight's energy conversion efficiency of a solar array.
- The power in orbit profile, that influences the overall EPS efficiency, as we will detail later.

Optimal Mean Delivered Power Configurations

Due to the monotone increasing relationship between the solar array area and the output power P_U, maximizing the mean delivered power P_{MEAN} for a given area A_{REQ} is equivalent to minimize solar array area for a given $P_{MEAN} = P_{REQ}$. The latter approach corresponds to the conventional design process, in whom the power required by all the loads drives the solar array area determination process [6].
Because of these considerations the problem of identifying the optimal solar array configuration can be stated as:

For a given orbit, selecting whatever value of a finite number of design parameters among a design space, find the solar array configuration that minimizes A_P, delivering at least P_{REQ} for every possible year's period.

From now on we will refer to A_{SA} as the A_P value that strictly satisfies the power requirement P_{REQ} in the year's worst case among equinoxes and solstices.
It can be stated that the configuration solution of the above problem is the sun pointing solar array, whose performances are obviously higher than all the others. In order to reduce the number of design alternatives, and therefore simplify the comparison between SP and BM configurations, a parametric analysis has been conducted on the A_{SA} of SP arrays. The parameters intervals considered in the analysis are:

- P_{REQ}; among 50, 100 and 150 [Watts]
- Rear side's surface finish; among Black Acrilic Paint, White Epoxy Paint and OSR Silvered Teflon.
- Cell Technology[3]; among Silicon, Gallium Arsenide Single, Double, Triple and Improved Triple Junction (ITJ).

For reference purposes the values used in the calculations for surface finishes and solar cell's characteristics are reported in Table 4 and Table 5.

[3] All solar cells considered come from the same manufacturer : SpectroLabs, Inc.

Surface Finish	Mean solar Absorptivity	Mean Infrared Emissivity
Black Acrilic Paint	0.975	0.874
White Epoxy Paint	0.248	0.924
OSR Silvered Teflon	0.077	0.790

Table 4 – Surfaces finish thermal characteristics [16].

Solar Cell	Nominal Efficiency (%) η_0	Temperature Coefficient (%) K_T
Silicon K6700B	13.7	-0.445
GeAs/Ge Single Junction	19.0	-0.164
$GaInP_2$/GaAs/Ge Dual Junction	21.5	-0.165
Triple Junction	24.5	-0.254
Improved Triple Junction (ITJ)	26.8	-0.227

Table 5 –Solar Cells Characteristics [8].

For every local time considered, the model identified in Section 2 has been applied and the obtained results show:

- Linear relationship between A_{SA} and P_{REQ}.
- Monotone behavior with increasing solar cell's technology.
- Little effects of rear side's surface finish on A_{SA}.

Figure 12 and Figure 13 illustrate some of these results.

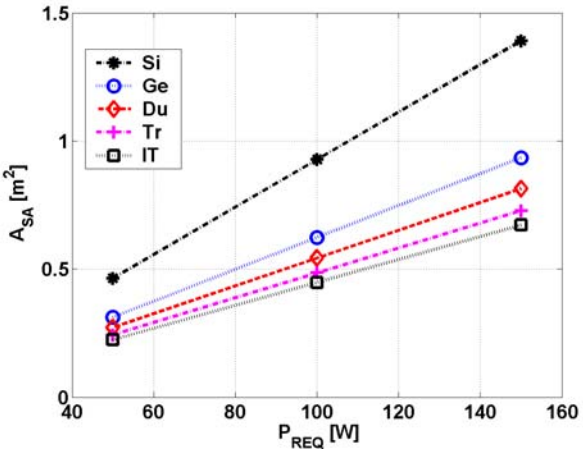

Figure 12 - A_{SA}–P_{REQ} for various Solar Cells.

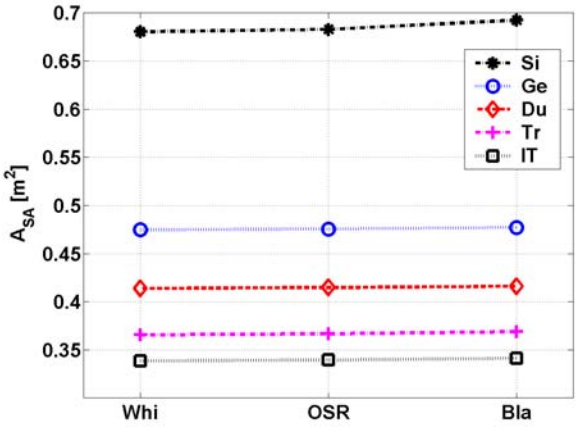

Figure 13 - A_{SA}–rear side material for various solar cells.

Due to the simple nature of the dependencies emerged, we can consider as meaningful for all the design space only one test case, i.e. one reference value of P_{REQ}, one kind of cell and one kind of surface finish. In detail, we will refer to a solar array of ITJ solar cells, whose rear side is covered with Black Acrilic Paint and designed to deliver a P_{REQ} of 100 W. Therefore, without loss of significance for all the other combinations of parameters, we can perform a comparative evaluation between sun pointing and body mounted configurations only on the selected test case.

Test Case Configurations Evaluation—Sun pointing solar panels are characterized by some considerable drawbacks, like reliability, continuous perturbations induced on satellite's attitude, more complex design and additional power consumption to orientate the panel and correct the attitude. On the other hand, fixed panels configurations have great advantages in terms of reliability, simplicity and, therefore, cost. BM configurations can be compared in terms of the A_{SA} excess of BM's w.r.t. SP. Thus, considering the SP configuration as the maximum attainable performance, let us define:

$$\delta A_{SP} \triangleq \frac{A_{SA|BM} - A_{SA|SP}}{A_{SA|SP}} \qquad (8)$$

Where $A_{SA|SP}$ and $A_{SA|BM}$ are the values of A_{SA} of the SP and BM configurations, accounting for all the panels used.
On the basis of the results of the analysis performed in Section 3, the following body mounted configurations, are selected:

- 1 BM – Only one panel, mounted on Anti-ω_{ORB} face.
- 3 BM – Three panels, mounted on Velocity, Anti-Velocity and Anti-Earth faces.
- 4 BM – Composition of 1 BM and 3 BM, i.e. Anti-ω_{ORB}, Velocity, Anti-Velocity and Anti-Earth.
- 5 BM – All available faces covered with panels, i.e. ω_{ORB}, Anti-ω_{ORB}, Velocity, Anti-Velocity and Anti-Earth.

Figure 14 collects the obtained A_{SA} values of each configuration in the local time range.

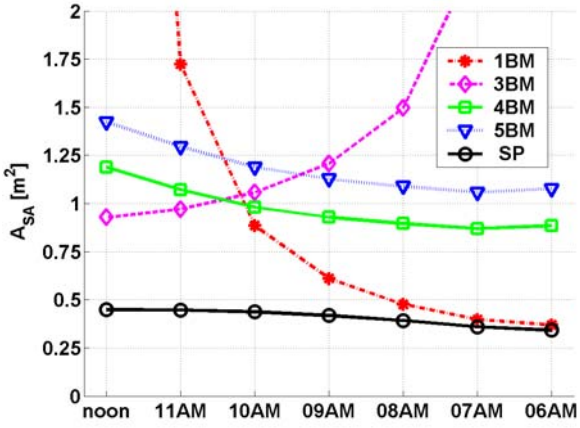

Figure 14 - A_{SA} values for various orbits and various configurations, P_{REQ} = 100 W.

The 3 BM configuration results optimal in the 12 and 11 am orbits, even if with high penalties w.r.t the corresponding $A_{SA|SP}$, mainly due to the perennial eclipse condition of at least one panel at a time. Moving towards 6 am orbits requests significant larger area for this kind of configuration. For the 10 am orbit, indeed, the larger A_{SA} compared to that of the 4 BM shows how the area increment caused by an increased number of panels is completely balanced by the loss of sunlight's energy conversion efficiency of the three Velocity, Anti-Velocity and Anti–Earth panels, that decreases to really small values at earlier local times.
The 1 BM configuration shows, instead, in the 6 and 7 am orbits, an excellent value of $A_{SA|BM}$, practically equal to $A_{SA|SP}$. It reveals also the smallest A_{SA} between BM configurations for local times earlier than 11 am.

Hence, the minimum A_{SA} criteria designates the 3 BM in the 12 and 11 am orbits as the less penalizing body mounted configuration w.r.t. an SP one. For all the other orbits the 1 BM is preferable between body mounted options. Table 6 collects the resulting minimum A_{SA} configurations with the corresponding values of $A_{SA|BM}$ and $A_{SA|SP}$.

Local Time	Minimum - A_{SA} Configuration	$A_{SA\|BM}$ [m^2]	$A_{SA\|SP}$ [m^2]
12 am	3 BM	0,929	0,449
11 am	3 BM	0,970	0,447
10 am	1 BM	0,886	0,437
9 am	1 BM	0,611	0,419
8 am	1 BM	0,475	0,392
7 am	1 BM	0,398	0,360
6 am	1 BM	0,368	0,342

Table 6 – Minimum A_{SA} BM configurations.

Figure 15 shows the values of δA_{SP}, that quantify, from the definition (8), the loss of performance of the computed optimal BM configurations w.r.t. SP ones.

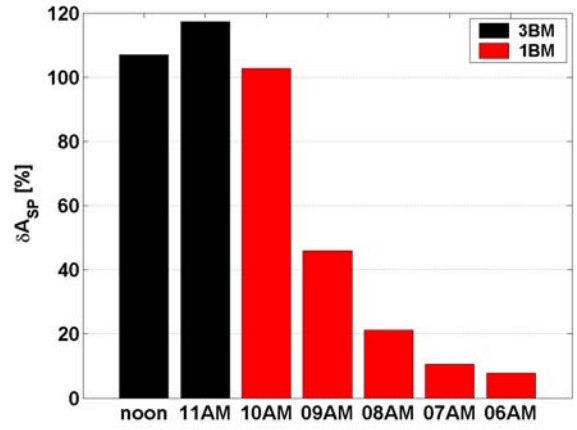

Figure 15 – δA_{SP} vs. Orbit for Minimum A_{SA} Configurations.

The choice of adopting a BM configuration instead of an SP one leads to a considerable raise in total solar cells area for local times from noon to 10 am. In these orbits waiving the active orientation of the solar array leads to roughly double the necessary solar cell area. Moving towards the 6 am ascending node local time, the A_{SA} increase, i.e. the performance reduction, becomes less significant, decreasing to less than 10 % in the dawn–dusk orbit. Hence, in 12 to 10 am orbits, pointing the solar array towards the sun gives great benefits in terms of the necessary solar cell area. Instead, moving towards 6 am orbits the performance gap of simpler BM configurations progressively reduces, and, thus, the choice of adopting a sun pointing array becomes less convenient.

The above considerations should be completed observing that BM configurations allocable solar cells area is limited by satellite's volume. Indeed, since the bus volume is determined in compliance with a relevant number of parameters besides electrical power requirements, fixing a BM configuration sets an upper limit on the allocable solar panel area. This limit softens, i.e. the maximum allocable solar panel area grows, as the number of panels foreseen by a BM configuration increases.
We can evaluate, for each minimum A_{SA} configuration, the "usefulness" associated with the decision of increasing the number of satellite's faces covered with solar panels. For fixed volume, this usefulness increases as the raise[4] in A_{SA} decreases. For constant A_{SA}, instead, the usefulness increases as the reduction in the volume needed to locate A_{SA} raises. Therefore, we can assume as an index of the convenience of the decision of increasing the number of panels of a minimum A_{SA} configuration, the ratio between the volume V decrease and the A_{SA} raise:

$$U_+ \triangleq \frac{V - V_+}{A_{SA+} - A_{SA}} \qquad (9)$$

Where the subscript + refers to the configuration with the added panels.
From the optimal BM configurations emerged in the above analysis (Table 6), it can be seen that increasing the number of panels leads to the 4 BM configuration in any considered local time. Hence, Figure 16 shows the values of U_+ in the 12 to 6 am orbits, for minimum A_{SA} configurations versus the 4 BM one.

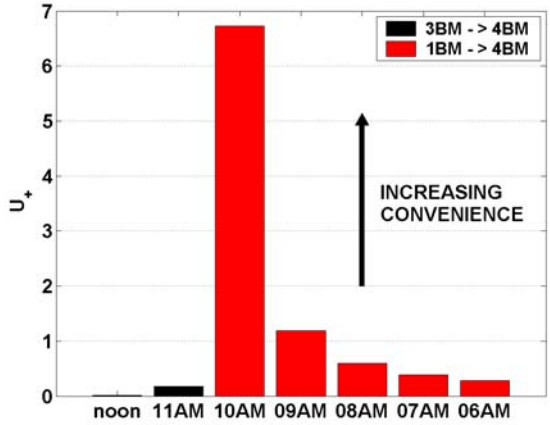

Figure 16 – U_+ vs. Orbit for Minimum A_{SA} Configurations.

In the 12 and 11 am orbit, there is little convenience to add the Anti-ω_{ORB} panel, mainly due to its poor performance[5]. In the 10 am one, the volume needed to locate the A_{SA} of a 4 BM configuration is significantly less than the corresponding 3 BM one, while the A_{SA} raise is limited. In this orbit, if the requested power P_{REQ} leads to $A_{SA|1BM}$ values conflicting with the volume constraint, the 4 BM configuration is surely preferable. From the resulting values of U_+, this effect weakens for earlier local times, still remaining bigger than in the 12 and 11 am orbits.
Hence, despite of the bigger A_{SA} values, the 4 BM configuration can result as optimal between body mounted arrays in 10 to 6 am orbits.

Optimal Power Time History

Since peaks in power output cannot be completely transferred to the load and/or battery charge, and because of the varying battery charge efficiency with the charge current, a uniform power output along the orbit daylight is desirable [3],[5].
Between power profiles with the same eclipse times, we can assume as index of non-uniformity in power output the

[4] Moving away from a minimum A_{SA} configuration surely produces an increase in A_{SA}.

[5] See Figure 9 to Figure 11

Standard Deviation (STD) of the daylight power time history w.r.t. its mean value. The eclipse time depends on the year period, attaining a maximum at the winter solstice in all the examined orbits. Therefore, the analysis has focused on power profiles at the winter solstice. From the results of the previous section, in each orbit three configurations are compared: the SP, the minimum A_{SA}[6] BM and the 4 BM.

The results are collected in Table 7 that reports also the season when the mean delivered power is minimum.

In the 12 and 11 am orbit the 3 BM configuration has a significant non-uniformity compared to that of the SP, and very similar to the 4 BM option. In the 10 to 6 am orbits, instead, the power profile of the 1 BM is closer to the one of SP. On the other hand, the 4 BM shows a significant higher non-uniformity, that is consequence of the power contribution of panels whose normal lies in the orbital plane. In the cases, outlined in the previous section, in whom the 4 BM could be preferable, this additional drawback should be taken into account, considering that the delivered energy is less exploitable.

		Configurations		
		Minimum A_{SA}	**SP**	**4 BM**
Local Times	**Noon**	153,3	153,4	153,3
		25,42	2,27	27,03
		sum.solstice	win.solstice	win.solstice
	11 am	157,2	152,8	152,9
		26,11	2,26	23,92
		sum.solstice	win.solstice	win.solstice
	10 am	150,2	150,1	150,3
		8,72	2,21	21,01
		win.solstice	win.solstice	win.solstice
	9 am	144,8	144,8	145,0
		6,12	2,05	19,04
		win.solstice	win.solstice	win.solstice
	8 am	136,5	136,5	136,5
		4,90	1,77	17,75
		win.solstice	win.solstice	win.solstice
	7 am	126,2	126,2	126,4
		4,14	1,54	16,78
		win.solstice	win.solstice	win.solstice
	6 am	120,1	120,1	124,6
		3,87	1,48	17,45
		win.solstice	win.solstice	equinoxes
		Cluster's Legend		
		Sunlight Average Power [W]		
		Standard Deviation [W]		
		Minimum Power Season		

Table 7 – In Orbit Power Mean Value and Standard Deviation.

[6] See Table 6 for the reference minimum–A_{SA} body mounted configurations.

Figure 17 shows the optimal configurations power profiles at winter solstice for 12, 9 and 6 am orbits.

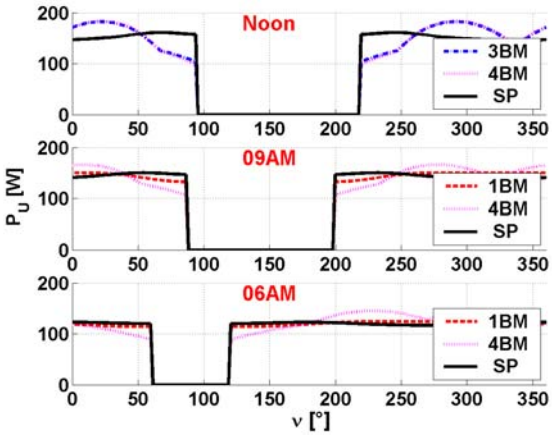

Figure 17 – Optimal Configurations Power Time Histories.

Configuration Comparative Evaluation

The previous analysis has identified three different solar array configurations per each examined orbit. Besides SP arrays, an optimal BM configuration has been defined. Its optimality is quantified by the necessary solar cells area and the power orbital profile uniformity, described by the Standard Deviation (STD) of the daylight power time history w.r.t. its mean value. Furthermore, the definition of an additional less volume-demanding BM configuration arises, that resulted to be the same in any local time. Specifically, as the alternative non area-optimal option, the 4 BM solar array is selected.

The comparison among these different options cannot be exhaustively solved unless system level issues and mission's contingent necessities are considered. To give general applicability to the performed analysis, only the performance difference between the various options is quantified, by means of the indexes (8),(9) and the comparison of the STD values.

Table 8 synthetically collects, in each local time, the most representative results for the three configurations.

Since only two BM configuration resulted as optimal in the local time interval, two corresponding kinds of orbits are distinguished. Specifically in the 12 and 11 am orbits, in which the 3 BM option is selected, due to the relevant δA_{SP} values and STD difference w.r.t SP, the choice of a body mounted configuration highly limits the attainable mission performances. In these orbits an SP solar array can be mandatory to achieve high performances with small satellite buses. The limited values of U_+ suggest that no significant benefits derive from adopting a 4 BM configuration to increase solar cells maximum allocable area for a given volume. It is worth highlighting that the significance of these
considerations increases moving from 12 am towards earlier local times.

In 9 to 6 am orbits a single panel body mounted array leads

to the minimum A_{SA} value. Again, the considerations that can be made are more significant for earlier local times. The δA_{SP} and STD values show that there is little convenience to adopt a more complex sun pointing solar array, because it leads only to a limited performance improvement. Since it foresees only one panel, the 1 BM configuration is high volume-demanding. Accepting a bigger solar cell area in order to have a volume reduction can be effective, especially in 9 am orbits. However, the less uniform power profile of the 4 BM w.r.t. the 1 BM configuration additionally reduces the performances attainable by such a type of solar array.

In the 10 am orbit, the results are intermediate between these two different kind of orbits, as Figure 14 and the δA_{SP} and STD values suggest. Since the δA_{SP} value resembles the 12 and 11 am ones, the corresponding considerations on the convenience of adopting a SP array are still applicable. Moreover, from inspection of Figure 14, the A_{SA} values of both 1, 3 and 4 BM configurations result very narrow, and, hence, the U_+ index reaches a maximum. Therefore, the selection of the optimal BM option is driven in these orbits by the maximum allocable solar cells area, i.e. the bus volume. However, comparing the 4 BM and 1 BM STD values points out that actually the latter is subject to significant higher energy-transfer losses, meaning that the 1 BM is still preferable, if no volume constraint is violated.

Local Time	Minimum A_{SA}			SP		4 BM	
	Config.	A_{SA} [m^2]	STD [W]	δA_{SP} (%)	STD [W]	U_+	STD [W]
Noon	**3 BM**	0,929	25,42	106,93	2,27	0,157	27,03
11 am	**3 BM**	0,970	26,11	117,22	2,26	0,181	23,92
10 am	**1 BM**	0,886	8,72	102,75	2,21	6,730	21,01
9 am	**1 BM**	0,611	6,12	45,86	2,05	1,192	19,04
8 am	**1 BM**	0,475	4,90	21,26	1,77	0,596	17,75
7 am	**1 BM**	0,398	4,14	10,62	1,54	0,383	16,78
6 am	**1 BM**	0,368	3,87	7,81	1,48	0,284	17,45

Table 8 - Solar Array Configurations Comparison.

5. CONCLUSIONS

A beginning of life maximum power point, solar array power output model has been developed. In order to correctly describe temperature effects on power output, various thermal models have been compared, selecting the better one in dependency from the solar panel type. Specifically, a constant temperature model has been selected for both deployed and body-mounted solar arrays. In the case of deployed arrays the reference temperature is evaluated averaging the steady-state temperature over the sunlit portion of the orbit. Whereas, steady-state temperature is averaged over the whole orbit period for body mounted arrays.

Then, body mounted solar arrays have been compared to sun pointing ones for sunsynchronous orbits as a function of the ascending node local time. In particular, body mounted configurations have been evaluated in terms of total area for a given energy requirement, in order to identify the best alternatives to sun pointing arrays. In this process, the area increment w.r.t. the optimal solution has been also computed, in order to verify if a limited penalty in terms of area could lead to a significant reduction in satellite volume. For ascending node local times ranging from 12 to 11 am, a body mounted configuration of three panels with normal vector lying in the orbital plane is optimal in terms of area. No significant advantages in terms of volume can be gained adding one more panel to this configuration. When the ascending node local time is within [10 am, 6 am], area is minimized by one panel with normal vector opposed to the orbit normal. For 10 am, adding three panels (with normal lying in the orbital plane) results in a 70% volume reduction at the expense of a 10% of solar array area increase. When moving towards 6 am the area disadvantage increases and the volume advantage decreases: at 6 am adding three panels results in a 9% volume reduction at the expense of a 140% of solar array area increase.

Area-driven optimal configurations are also analyzed in terms of uniformity of power generation. This parameter is quantified by the standard deviation of solar array generated power along the sunlit portion of an orbit at winter solstice. It decreases from noon (about 17%) to six am (about 3%). No advantage in uniformity is obtained by selecting a 4 panel configuration.

If optimal body mounted configurations are compared to a sun pointing solar array which meets the same energy requirement, a disadvantage can be envisaged in terms of area. In particular, using body mounted panels on 12 to 10 am orbits practically doubles the required area. For 9 am orbits the increase is about 50%, reducing to 8% in 6 am. Of course, a final decision between body mounted and sun pointing arrays must weigh system-level requirements in terms of cost and reliability.

For the analysis to be complete, deployable, non actively orientated arrays should be studied. It is worth noting that several issues arise. First of all, thermal model must be analyzed and, depending on the configuration, shadowing effects considered. In addition, deployment angles and their constraints must be included in the design variables to be optimized.

REFERENCES

[1] H. Steyskal,, J.K. Schindler, P. Franchi, R.J. Mailloux, *2001. Pattern Synthesis for TechSat21 – A Distributed Space-Based Radar System*. Proceedings of the 22nd IEEE Aerospace Conference, Vol. 2, pp. 725-732.

[2] Massonnet, *IEEE TGRS*, Vol. 39, No. 3

[3] D'Errico, M., and M. Pastena, 1998. *Solar Array Design and Performance Evaluation for the SMART Microsatellite*, 49th Congress of the International Astronautical Federation, Sept. 28-Oct. 2, Melbourne, Australia (paper IAF-98-R.1.06).

[4] M.Fragnito, M. Pastena, and M. D'Errico, 2002. *Spacecraft Thermal Analysis and Control by Thermal Energy Optimum Distribution*, AIAA Journal of Spacecraft and Rockets, Vol. 39, No. 1, pp. 149-152.

[5] P.A.Anigstein, and R. S. Sanchez Peña, 1998. *Analysis of Solar Panel Orientation in Low Altitude Satellites*. IEEE Transactions on Aerospace and Electronic Systems, Vol. 34, No. 2, pp. 569-578.

[6] J.R.Wertz, and W.J. Larson, 1991. *Space Mission Analysis and Design*, Kluwer Academy Publishers, Boston MA.

[7] H.S.Rauschenbach, *Solar Cell Array Design Handbook,* JPL SP 43-38, Vol. 1, 1976

[8] *Spectrolab Inc. Products Data Sheets*.

[9] A.Capel, P. Chapoulie and S. Zimmermann, *Dynamic Performance Simulation of a Spacecraft Power System,* Sixth European Space Power Conference Proceedings, May 6-10, 2002

[10] D. Loche, POWER-SYSTEMA: *The Next Generation of Power Simulator*, Sixth European Space Power Conference Proceedings, May 6-10, 2002

[11] C. Hampe, A. Löffler & D. Reggio, *Real-Time Simulation of a Satellite's Electrical Power System*, Sixth European Space Power Conference Proceedings, May 6-10, 2002

[12] T.W.Kerslake, F.M.Haraburda and J.P.Riehl, *Solar Power System Options for the Radiation and Technology Demonstration Spacecraft*, IEEE AES Systems Magazine, February 2001

[13] T.W.Kerslake and L.P.Gefert, *Solar Power System Analyses for Electric Propulsion Missions*, IEEE AES Systems Magazine, January 2001

[14] R.L.Moser, *Electrical Power Subsystem Initial Sizing,* IEEE AES Systems Magazine, December 1990

[15] Y.Wang and M.Maier, *SEDSAT Solar Array Output Power Analysis*, Thirtieth Southeastern Symposium on System Theory Proceedings, March 8-10, 1998

[16] D.G. Gilmore, 1994. *Satellite Thermal Control Handbook* , The Aerospace Corporation Press, El Segundo CA.

[17] M.Fragnito and M.Pastena, *Design of SMART Microsatellite Deployable Solar Wings*, Acta Astronautica, Vol. 46, 2000.

[18] E. Van Den Berg and M. Kroon, *Algorithms and Performance of a Space Dedicated Solar Array Modelling Tool*, Sixth European Space Power Conference Proceedings, May 6-10, 2002

[19] B.N.Agrawal, *Design of Geosynchronous Spacecraft*, Prentice-Hall, May 1986.

Urbano Tancredi *was born in 1976 and received the M.S. in Aerospace Engineering in 2001 from the University of Naples "Federico II". In the same year he joined the Italian Center of Aerospace Research as a Research Fellow. From 2002 he is attending a Ph.D. course in Aerospace Science and Technologies at the Second University of Naples. He is member of the scientific committee of CORISTA consortium, aimed at sensor development. His main field of activity is mission analysis of Earth observation systems and design of electrical power system for microsatellites.*

Marco D'Errico *was born in 1966 and received the M.S. in Aeronautical Engineering in 1992 and the Ph.D. in Aerospace Engineering in 1995, both from the University of Naples "Federico II". In 1995 he joined the Second University of Naples as assistant professor to become associate professor in 2000. He is member of the scientific committee of CORISTA consortium, aimed at sensor development. His main field of activity is mission analysis of Earth observation systems and design of electrical power system for microsatellites.*